Influence of mineralogy on the preservation of amino acids under simulated Mars conditions

Journal Item

Icarus 277 (2016) 342–353

Contents lists available at ScienceDirect

Icarus

journal homepage: www.elsevier.com/locate/icarus

Influence of mineralogy on the preservation of amino acids under simulated Mars conditions

Renato dos Santos[a], Manish Patel[b,c], Javier Cuadros[d], Zita Martins[a,*]

[a] Department of Earth Science and Engineering, Imperial College London, South Kensington Campus, London SW7 2AZ, UK
[b] Department of Physical Sciences, The Open University, Milton Keynes MK7 6AA, UK
[c] Space Science and Technology Division, Rutherford Appleton Laboratory, Harwell, Oxfordshire, UK
[d] Department of Earth Sciences, The Natural History Museum, London SW7 5BD, UK

ARTICLE INFO

Article history:
Received 14 December 2015
Revised 18 May 2016
Accepted 19 May 2016
Available online 27 May 2016

Keywords:
Mars
Mineralogy
Solar radiation

ABSTRACT

The detection of organic molecules associated with life on Mars is one of the main goals of future life-searching missions such as the ESA-Roscosmos ExoMars and NASA 2020 mission. In this work we studied the preservation of 25 amino acids that were spiked onto the Mars-relevant minerals augite, enstatite, goethite, gypsum, hematite, jarosite, labradorite, montmorillonite, nontronite, olivine and saponite, and on basaltic lava under simulated Mars conditions. Simulations were performed using the Open University Mars Chamber, which mimicked the main aspects of the martian environment, such as temperature, UV radiation and atmospheric pressure. Quantification and enantiomeric separation of the amino acids were performed using gas-chromatography-mass spectrometry (GC–MS). Results show that no amino acids could be detected on the mineral samples spiked with 1 μM amino acid solution (0.1 μmol of amino acid per gram of mineral) subjected to simulation, possibly due to complete degradation of the amino acids and/or low extractability of the amino acids from the minerals. For higher amino acid concentrations, nontronite had the highest preservation rate in the experiments in which 50 μM spiking solution was used (5 μmol/g), while jarosite and gypsum had a higher preservation rate in the experiments in which 25 and 10 μM spiking solutions were used (2.5 and 1 μmol/g), respectively. Overall, the 3 smectite minerals (montmorillonite, saponite, nontronite) and the two sulfates (gypsum, jarosite) preserved the highest amino acid proportions. Our data suggest that clay minerals preserve amino acids due to their high surface areas and small pore sizes, whereas sulfates protect amino acids likely due to their opacity to UV radiation or by partial dissolution and crystallization and trapping of the amino acids. Minerals containing ferrous iron (such as augite, enstatite and basaltic lava) preserved the lowest amount of amino acids, which is explained by iron (II) catalyzed reactions with reactive oxygen species generated under Mars-like conditions. Olivine (forsterite) preserved more amino acids than the other non-clay silicates due to low or absent ferrous iron. Our results show that D- and L-amino acids are degraded at equal rates, and that there is a certain correlation between preservation/degradation of amino acids and their molecular structure: alkyl substitution in the α-carbon seem to contribute towards amino acid stability under UV radiation. These results contribute towards a better selection of sampling sites for the search of biomarkers on future life detection missions on the surface of Mars.

1. Introduction

The detection of organic molecules associated with extra-terrestrial life has been primarily focused on Mars due to its proximity to Earth, evidences of a congenial past environment and potential to support microbial life (Westall et al., 2013). Increasing evidence from NASA's *Opportunity* and *Curiosity* rovers obtained at different locations indicates that the Red Planet could have indeed supported life at the surface in the past (Arvidson et al., 2014; Grotzinger et al., 2014). Furthermore, the detection of silica-rich deposits by the Spirit rover in the Gusev crater is also an indication of an environment able to support life (Des Marais 2010; Ruff et al., 2011; Squyres et al., 2008). It is also plausible that life developed underground and biomarkers reached the surface (Michalski et al., 2013). Despite this, the environmental conditions that prevail now on Mars' surface are not congenial to life or to the preservation of biomarkers. Two of the factors contributing to the harsh current martian environmental conditions are the thin atmosphere and the absence of a significant magnetosphere (Fairén

* Corresponding author.
E-mail address: z.martins@imperial.ac.uk (Z. Martins).

http://dx.doi.org/10.1016/j.icarus.2016.05.029

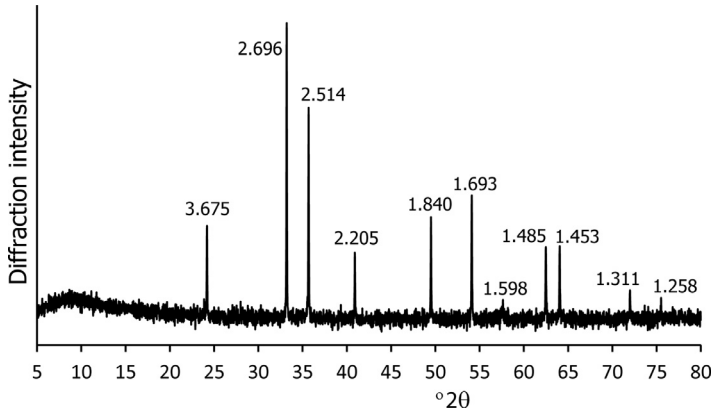

Fig. 1. Powder X-Ray diffraction patterns of hematite (Fe_2O_3). The figures indicate the d-spacing of the several peaks in angstroms. The intensity increase at ~10 °2θ is produced by the X-ray fluorescence of Fe.

et al., 2010), resulting in the inability to attenuate the intensity of the multiple forms of solar radiation that reach the planet, such as UV radiation, galactic cosmic rays and solar energetic particles (Cockell et al., 2000; Hassler et al., 2014). As a result, the martian regolith is exposed to intense levels of radiation, contributing to the reactivity of the soil which may destroy potential martian life and degrade organic molecules (Dartnell et al., 2007; Quinn et al., 2013). UV radiation leads to the formation of radical species (e.g. reactive oxygen species such as superoxide and hydroxyl radicals) by photochemical processes, which cause degradation of any potential organic compounds present on Mars (Benner et al., 2000; Georgiou et al., 2007, Georgiou et al., 2015; Yen et al., 2000). Amino acids, which are the building blocks of proteins and considered important target molecules in future life-searching missions (Parnell et al., 2007), are known to be subjected to degradation by UV radiation (Garry et al., 2006; Noblet et al., 2012). A 1.5-year exposure of glycine and serine to Mars-like surface UV radiation conditions in low-Earth orbit resulted in complete degradation of these organic molecules (Noblet et al., 2012).

In order to maximize the chances of finding biomarkers on Mars, we must determine the most suitable conditions to preserve them. Preservation of organic molecules on Mars is thought to be favored in subsurface environments, and also through associations with specific minerals that may confer protection from the harsh surface conditions (Kminek and Bada, 2006; Summons et al., 2011, and references therein; Poch et al., 2015). Despite the unfavorable conditions that are found at the surface, indigenous chlorinated hydrocarbons were recently detected on Mars by the Sample Analysis at Mars (SAM) instrument on-board Curiosity (Freissinet et al., 2015). The successful detection of organic molecules on samples from Mars' surface exposed to ionizing radiation and oxidative conditions suggests that: 1) the preservation of organic molecules may not be limited to subsurface environments, and 2) organic biomarkers may be found on the surface if associated with specific minerals.

In this paper we examine the preservation under simulated Mars-like conditions of amino acids that were spiked onto 11 minerals and onto basaltic lava, which are all present on the martian surface (Ehlmann and Edwards, 2014). The simulations were performed using a custom-built Mars environmental simulation chamber at the Open University (OU), Milton Keynes, UK. This facility permits multiple aspects of the martian environment to be simulated, including temperature, UV radiation, atmospheric pressure and composition. Analyses of the amino acids extracted from the mineral surfaces after the experiments were performed by gas chromatography-mass spectrometry (GC-MS). Our results are particularly relevant for future in situ life-detection missions, such as the ESA-Roscosmos ExoMars 2018 rover and the NASA Mars 2020 mission, highlighting which minerals may be the most suitable to protect amino acids from the harsh environmental conditions found at the martian surface.

2. Materials and methods

2.1. Minerals and XRD characterization

Eleven mineral samples were used in this work: augite (A), enstatite (E), goethite (G), gypsum (Gy), hematite (H), jarosite (J), labradorite (L), montmorillonite (M), nontronite (N), olivine (O) and saponite (S). Basaltic lava (B) was also used. They were all selected as representing abundant mineral phases on Mars (Ehlmann and Edwards, 2014). Augite, jarosite, labradorite, nontronite, and saponite were purchased from Richard Tayler (http://richardtayler.co.uk, Cobham, Surrey, UK). Enstatite, goethite and olivine were obtained from the Natural History Museum collection (NHM, London), all of them unregistered specimens in the NHM collection. The basaltic lava is a specimen collected in Mauna Loa (Hawaii) at the point of lava quenching and donated by Joe Michalski. Gypsum and hematite were purchased from Sigma Aldrich. The montmorillonite is SAz-1 (smectite-rich rock of volcanic origin) described in Cuadros (2002).

Minerals were ground to powder by hand with a mortar and pestle and they were analyzed with X-ray diffraction (XRD) at the NHM, in order to determine their purity and structure. They were side-loaded to avoid preferred orientation of particles and analyzed in the range 3–80° 2θ using a PANanalytical X'Pert Pro diffractometer operated at 45 kV and 40 mA, with Cu Kα radiation, divergence slit of 0.25°, Soller slits of 1.146° and a solid-state X'Celerator detector covering an angle of 2.1°. The basaltic lava contains the following mineral phases in the estimated order of abundance: volcanic glass, pyroxene, olivine, and labradorite. Jarosite is of the natrojarosite variety. Olivine is forsterite. The augite and enstatite contain some traces of amphibole; the nontronite and montmorillonite contain traces of quartz; the other minerals are pure at the XRD detection level. Fig. 1 shows the X-ray pattern of hematite as an example.

2.2. Chemicals and tools

The pipette tips and eppendorfs used in this work were bought sterile. Hydrochloric acid (37 wt. %), and high performance liquid chromatography (HPLC)-grade water were purchased from Sigma-Aldrich. Sodium hydroxide was purchased from Riedel-de Haen. Aluminium hydroxide and 2-aminoheptanoic acid (>97%) were purchased from Fluka. AG 50W-X8 resin (100–200 mesh) was acquired from Bio-Rad. HPLC-grade dichloromethane (DCM) was

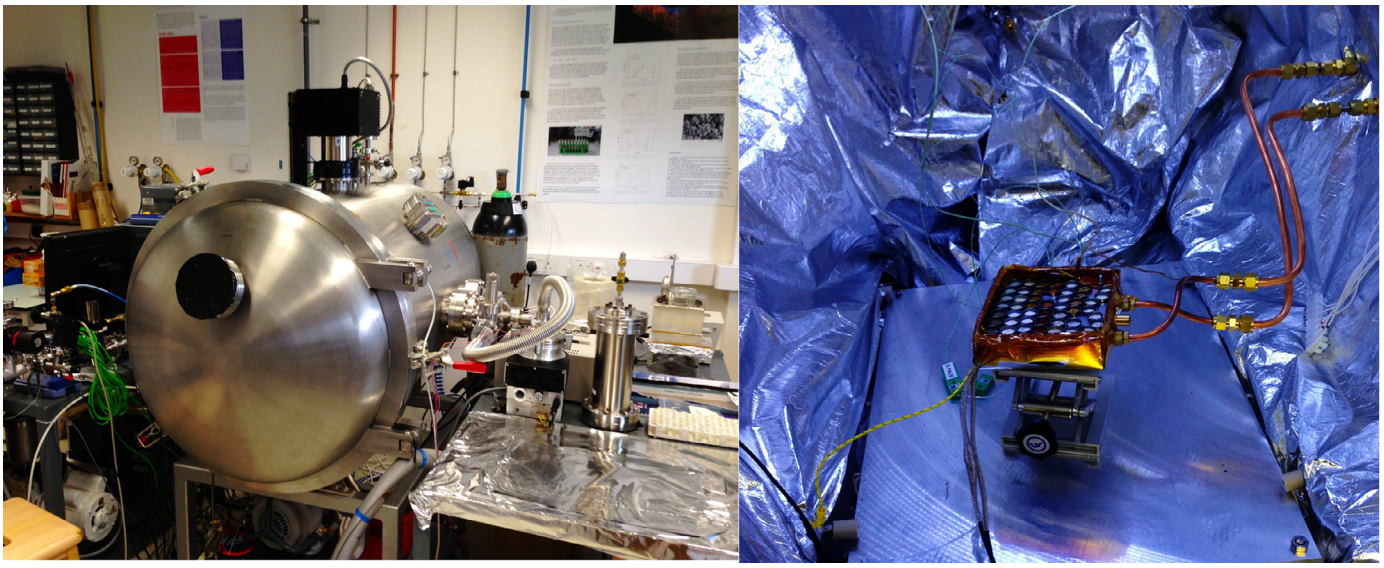

Fig. 2. Mars Chamber simulator located at the Open University (left) and the experimental setup inside the chamber showing the amino acid-spiked minerals (right).

purchased from Fisher Scientific. Copper turnings used for sulfur removal were purchased from BDH. The 25 amino acids used in the experiments were: α-aminoisobutyric acid (α-AIB); D,L-isovaline; D,L-alanine; D,L-valine; glycine; D,L-norvaline; D,L-β-aminoisobutyric acid (D,L-β-AIB); D,L-β-aminobutyric acid (D,L-β-ABA); β-alanine; D,L-leucine; D,L-norleucine; γ-aminobutyric acid (γ-ABA); D,L-aspartic acid; D,L-glutamic acid and 6-aminohexanoic acid (6-AHA). The amino acid L-2-aminoheptanoic acid (L-2-AHA) was not subjected to the simulation experiments and was used as internal standard for the GC-MS analysis. All the amino acid standards were purchased from Sigma-Aldrich, except D,L-isovaline, which was bought from Acros Organics. The trifluoroacetic anhydride isopropanol (TFAA-IPA) derivatization kit was obtained from Alltech. All glass tools and ceramics used were sterilized by wrapping in aluminum foil and heating in a furnace for at least 3 h at 500 °C.

2.3. Spiking of amino acids

A stock solution of 0.005 M concentration was prepared for each of the 25 amino acids. One milliliter of each amino acid stock solution was used to prepare a spiking solution containing an equimolar mixture of the 25 amino acids. Four of these solutions were prepared with final concentrations of 50, 25, 10 and 1 μM of each amino acid. The spiking solutions containing 1, 10, 25 and 50 μM concentrations of each amino acid were labeled as solution 1, 2, 3 and 4, respectively. Concentrations were chosen by adapting the protocols from Parbhakar et al (2007) and Cuadros et al. (2009). These authors show that at low amino acid concentrations the mechanism of amino acid adsorption on smectite is a simple exchange with interlayer cations, whereas at higher amino acid concentration physical interaction between amino acid molecules become important. In the present work we wanted to be in the low-amino acid concentration (i.e. much lower than 0.025 M) in order to avoid amino acid interaction with other amino acids.

Approximately 30 mg of each mineral sample described in Section. 2.1 were weighed in Pyrex test tubes. Three milliliters of each of the solutions described above (1–4) were transferred into 12 test tubes, each containing one of the minerals.

The experiments containing the minerals and the spiking solutions were named by the respective mineral initial provided in Section. 2.1, followed by the number of the solution. For example, augite spiked with solution 1 (i.e., 1 μM of each amino acid) was labeled as A1, while augite samples labeled as A2, A3 and A4 were spiked with solution 2, 3 and 4, respectively. Using this labeling procedure, the experiments carried out include basaltic lava (with experiments B1, B2, B3 and B4), enstatite (E1, E2, E3 and E4), goethite (G1, G2, G3 and G4), gypsum (Gy1, Gy2, Gy3 and Gy4), hematite (H1, H2, H3 and H4), montmorillonite (M1, M2, M3 and M4), nontronite (N1, N2, N3 and N4), olivine (O1, O2, O3 and O4) and saponite (S1, S2, S3 and S4). Jarosite was only used in experiments 3 and 4, resulting in a total of two samples (J3 and J4). Labradorite was only used in experiments 1, 2 and 3 (L1, L2 and L3).

All the test tubes containing the mineral samples and the spiking solutions were flame sealed and placed in an orbital shaker (Heidolph Polymax 1040) for 24 h at 50 revolutions per minute (rpm) in order to let amino acids adsorb onto the mineral surfaces. The outside of the test tubes was rinsed with HPLC grade water and cracked open. The content of the test tubes was dried under a flow of nitrogen (i.e., the spiking solution was dried in contact with the mineral). Thus, the 1, 10, 25 and 50 μM solutions correspond to 0.1, 1, 2.5 and 5 μmol/g of the amino acids on the minerals, respectively.

Control experiments were prepared by repeating the same procedure described in this section with a second set of samples. The first set of samples was used to perform the Mars chamber simulations, while the second set was used as controls (i.e., samples that were spiked but not subjected to the Mars simulation).

2.4. Mars chamber simulations

The spiked mineral standards were transferred into 14 mm diameter metallic sample cups and placed inside a Mars chamber simulator at the Open University, Milton Keynes, UK (Fig. 2). The sample cups were pre-sterilized by heat at 500 °C for 4 h. The thickness of the deposits was approximately 1 mm in order to avoid any self-shielding issues. The sample cups were placed on a custom-made cold plate, to enable the cooling of the samples to Mars-relevant temperatures. Copper shielding was provided to the edges of the plate to define a cold zone, and the external faces of the plate and shields were insulated to provide an efficient sample cooling zone. The cooling plate was connected to a liquid nitrogen supply, with thermal valves providing control over the sample

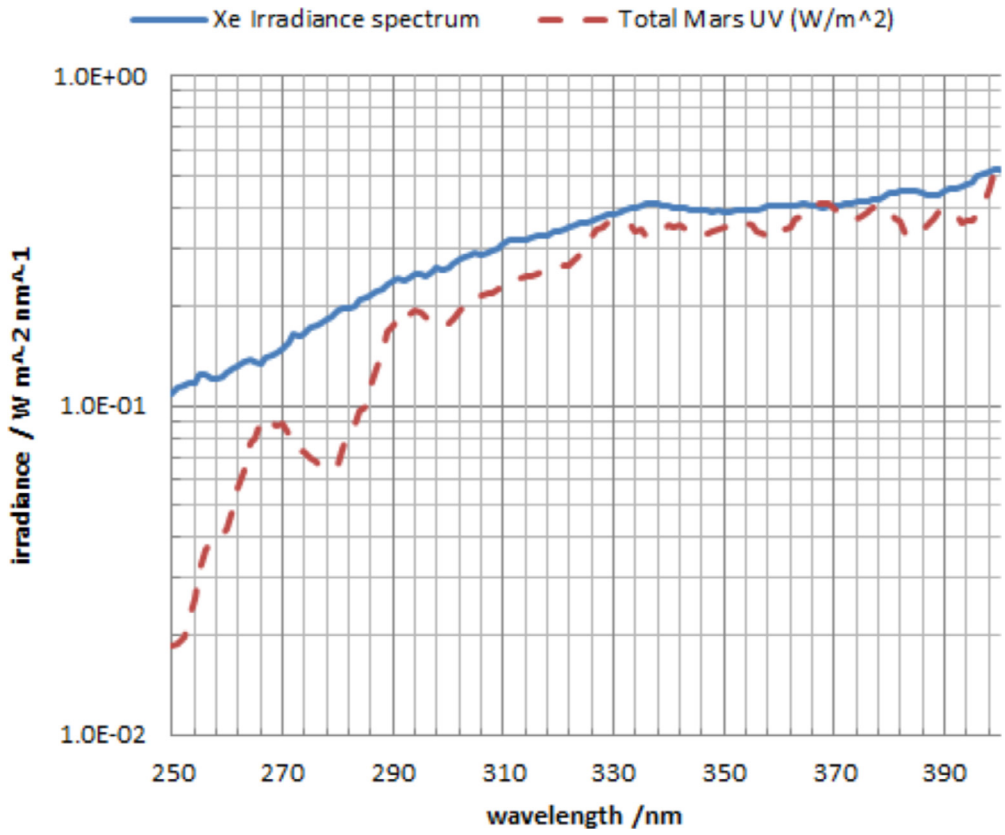

Fig. 3. UV lamp spectrum and modeled UV spectrum expected at the martian surface.

temperature. Temperature was monitored using an array of thermocouples mounted on the sample plate. The resulting sample configuration is shown in Fig. 2 (right). The chamber contained a Xe light source at the top of the chamber using a fused silica window (to ensure good UV transmission) providing direct illumination of the sample area with a UV spectrum similar to that encountered on the surface of Mars (e.g. Patel et al., 2002). The lamp output, along with a typical modeled UV irradiance expected at the surface of Mars at local noon (taken from Patel et al., 2002) is shown in Fig. 3. After setting the samples in the chamber and previous to the experiments, the pressure was reduced to a vacuum (<1 mbar) for >10 min and at room temperature. This ensures that there is no air and no water vapor in the atmosphere. Then, the chamber was pressurized at 6 mbar with a mixture of 95% CO_2 and 5% N_2, mimicking the approximate Mars pressure environment. The very dry conditions established by the initial vacuum treatment and the simulated Mars atmosphere (water vapor partial pressure is nominally zero) eliminated adsorbed water from the mineral surfaces. Complete removal of adsorbed water is likely not obtained, unless the samples are sufficiently heated. Thermal cycling of the sample (to simulate the potential diurnal thermal cycle of Mars, e.g. Kieffer et al., 1977) was performed, with a cycle from −80 °C to +20 °C of 2 h duration repeated throughout the exposure. During thermal cycling the samples were exposed to UV, and overnight the samples were maintained at room temperature with no UV. The samples received a total of 28 h of real-time continuous UV illumination. On Mars, the diurnal profile of UV irradiance encountered at the surface exhibits a bell-shaped profile (such as demonstrated in Patel et al., 2002), therefore the local noon irradiance represents a peak irradiance and the UV levels throughout the rest of the day are significantly lower. Given the higher irradiance level of the lamp as shown in Fig. 3, coupled with the effect of a diurnal light curve profile, the lab irradiance of 28 h is calculated to correspond to a martian equivalent UV dose of approximately 6.5 days. Upon completion, the chamber was restored to ambient conditions before removal of the samples from the chamber.

2.5. Extraction, derivatization and GC-MS analyses of amino acids

After the Mars simulation, amino acids were extracted from the minerals and derivatized according to the procedure described by Martins et al. (2011, 2015 and references therein). A step to remove sulfur was performed between the desalting and derivatization, by using copper turnings (activated in a 10% HCl solution). The activated copper turnings were added to V-vials containing the desalted amino acid sample residues, brought up with 1 mL of HPLC grade water, and left overnight. The copper turnings were then removed and the V-vials were dried under a flow of N_2. The derivatized amino acids were dissolved in 75 μL of DCM.

The GC-MS analyses were performed using a Perkin Elmer Clarus 580 gas chromatograph/Clarus SQ 8S mass spectrometer. The amino acids were separated using two Agilent Chirasil L-Val capillary columns (each 25 m, inner diameter 0.25 mm, film thickness 0.12 μm) connected by a zero dead-volume connector. Helium was used as carrier gas with a 1 mL/min flow. GC injector temperature was set at 220 °C. Automatic splitless mode was used for injection and the oven programme was: 1) 35 °C for 10 min; 2) 2 °C per minute increase until 80 °C, hold for 5 min; 3) 1 °C per minute increase until 100 °C; and 4) 2 °C per min increase until 200 °C, hold for 10 min (total run time 117.5 min). Temperatures for the transfer line and the MS ion source were set at 220 °C and 230 °C, respectively.

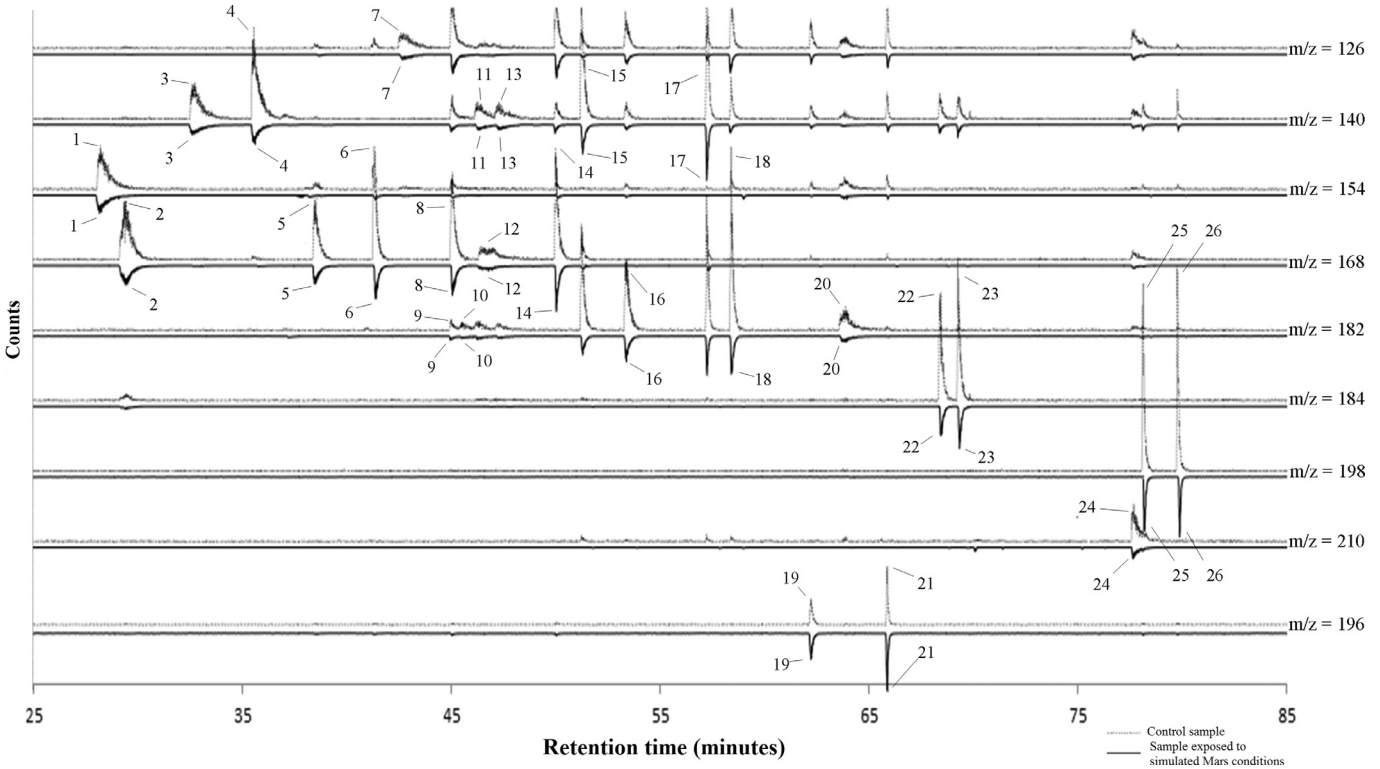

Fig. 4. Single ion GC-MS chromatograms (25 to 85 min) of the derivatized (N-TFA, O-isopropyl) amino acids extracted from control sample G4 (goethite spiked with solution 4, but not subjected to the Mars simulation; chromatograms pointing upwards) and corresponding sample G4 (goethite spiked with solution 4 and analyzed after the Mars chamber simulations; chromatograms pointing downwards). All single ions chromatograms are in the same scale. 1) α-AIB; 2) D,L-isovaline; 3) D-alanine; 4) L-alanine; 5) D-valine; 6) L-valine; 7) glycine; 8) D-norvaline; 9) D-β-AIB; 10) L-β-AIB; 11) D-β-ABA; 12) β-alanine; 13) L-β-ABA; 14) L-norvaline; 15) D-leucine; 16) D-norleucine; 17) L-leucine; 18) L-norleucine; 19) D-2-aminoheptanoic acid (internal standard); 20) γ-ABA; 21) L-2-aminoheptanoic acid (L-2-AHA, internal standard); 22) D-aspartic acid; 23) L-aspartic acid; 24) 6-AHA; 25) D-glutamic acid; 26) L-glutamic acid.

The identification of amino acids was achieved by comparing the retention times and mass fragmentation patterns of the amino acids present in the samples with those obtained from known amino acid standard mixtures. The amino acid detection limit of the GC-MS was verified to be approximately 3 parts per billion (ppb). Typical GC-MS chromatograms from simulated G4 sample and respective control are provided in Fig. 4. Amino acids were quantified by peak area integration of the corresponding ion fragment, which were then converted to abundances using calibration curves. These were created by plotting the ratio of the amino acid standard/internal standard target ion peak area versus the mass of amino acid standard injected into the column.

2.6. Brunauer–Emmett–Teller (BET) analyses

Brunauer–Emmett–Teller (BET) analyses were performed to measure the surface area and pore size of the 11 minerals and basaltic lava used in this work. These two variables are likely to be the most relevant for amino acid adsorption and protection from UV radiation because they have an important control on amino acid distribution and arrangement on the mineral surface and on physical shielding. Prior to analysis, approximately 0.5 g of all samples were outgassed overnight at 353 K, under high vacuum. Measurements were performed using a Micrometrics TriStar 3000 gas adsorption analyzer, using N_2 as adsorptive gas. Measurements were made in the relative pressure (P/P_0) range from 0.01 up to 0.99. Final results were calculated using 9 equilibrium points in the P/P_0 range between 0.03 and 0.20 (all linear regressions had a correlation coefficient higher than 0.999).

3. Results

3.1. Degradation of amino acids under simulated Mars conditions

The fraction of extractable amino acids preserved after exposition to simulated Mars surface conditions was calculated as the ratio A/A0 (%), where A is the amount of each amino acid that was not degraded and successfully extracted after the Mars Chamber experiment, and A0 is the total amount of amino acid extracted from the correspondent control (i.e., equivalent samples, prepared in the same conditions, but not exposed in the Mars Chamber). The amount of the amino acids extracted from the controls is an effective way to ascertain whether a lack of detection of amino acids in a tested sample is due to degradation or to low extraction. The lack of amino acid detection in both exposed sample and correspondent control suggests that the lack of detection in the former cannot be attributed to degradation induced by the simulated martian environmental conditions.

The fractions of amino acids extracted from the control samples (i.e. [A0]/initial amino acid in the spiking solution) were calculated. They ranged from 0 (no amino acids were detected in augite A1, basalt lava B1 and nontronite N1) to 86%, 13 to 100%, 0 to 96%, and 0 to 92% for experiments 1, 2, 3, and 4, respectively. Fig. 5 shows the average A/A0 ratios (in %) obtained for the 25 amino acids that were used in experiments 2, 3 and 4. These values were calculated from the individual A/A0 (%) obtained for each of the 25 amino acids (individual A/A0 ratios are shown in Tables 1–3).

Results from experiment 1 (i.e., minerals spiked with solution containing 1 μM of each amino acid; not presented) show that no amino acids were detected in any of the exposed samples (the amino acid detection limit of the GC-MS is ~3 ppb). In the con-

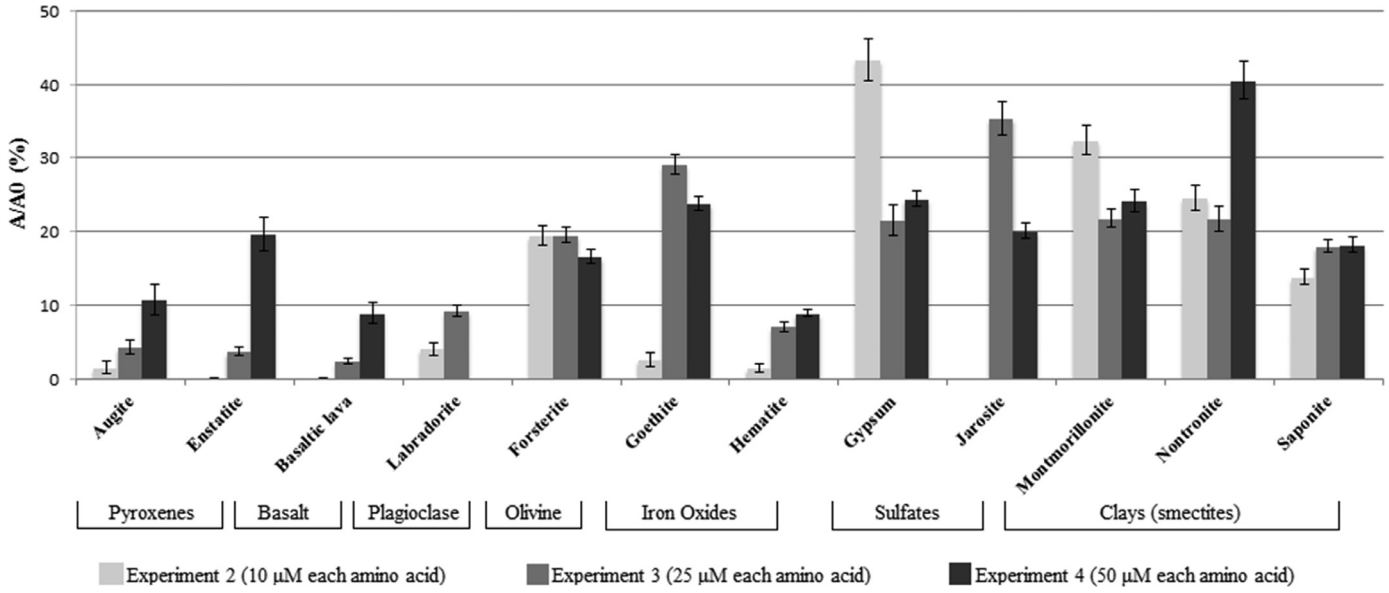

Fig. 5. Summary of the average A/A0 amino acid ratios (in %) obtained after the simulation experiments in the Mars Chamber, where A is the amount of amino acids that were not degraded and extracted after the simulation, and A0 is the total amount of amino acids extracted from the corresponding controls. Average values presented in this figure were calculated using all the A/A0 ratios obtained for each of the 25 amino acids that were spiked in a given experiment found in Tables 1–3. The lack of bars in basaltic lava and enstatite for experiment 2 means complete degradation of amino acids. Labradorite and jarosite were not used in experiments 4 and 2, respectively.

Table. 1
Summary of the individual A/A0 ratios (in %) obtained for experiment 2 (spiking solution, 10 μM of each amino acid) where A is the amount of the remaining amino acids detected in simulated samples and A0 is the amount of amino acids detected in the control.

Individual amino acid (A/A0) vs mineral	Augite (A2)	Basaltic lava (B2)	Enstatite (E2)	Goethite (G2)	Gypsum (Gy2)	Hematite (H2)	Labradorite (L2)	Montmorillonite (M2)	Nontronite (N2)	Olivine (O2)	Saponite (S2)
α-AIB	3 ± 1	0[a]	0[a]	9 ± 0	17 ± 1	0[a]	0[a]	42 ± 4	18 ± 2	22 ± 1	18 ± 7
D,L-isovaline[b]	3 ± 1	0[a]	0[a]	7 ± 0	12 ± 1	5 ± 2	0[a]	34 ± 3	12 ± 1	14 ± 1	14 ± 5
D-alanine	0[a]	0[a]	0[a]	0[a]	24 ± 2	0[a]	0[a]	40 ± 4	25 ± 2	16 ± 1	19 ± 6
L-alanine	0[a]	0[a]	0[a]	0[a]	20 ± 2	0[a]	0[a]	34 ± 3	22 ± 2	16 ± 2	15 ± 5
D- valine	2 ± 0	0[a]	0[a]	4 ± 0	32 ± 2	3 ± 0	9 ± 1	30 ± 2	18 ± 2	14 ± 1	15 ± 5
L- valine	2 ± 0	0[a]	0[a]	5 ± 0	30 ± 1	4 ± 1	8 ± 0	31 ± 2	19 ± 1	13 ± 1	12 ± 4
glycine	0[a]	0[a]	0[a]	0[a]	54 ± 4	0[a]	0[a]	68 ± 5	51 ± 5	22 ± 1	18 ± 5
D- β- AIB	0[a]	0[a]	0[a]	0[a]	49 ± 2	0[a]	0[a]	32 ± 3	29 ± 3	26 ± 3	0[a]
L- β- AIB	0[a]	0[a]	0[a]	0[a]	48 ± 5	0[a]	0[a]	35 ± 5	24 ± 4	26 ± 2	0[a]
D- β- ABA	0[a]	0[a]	0[a]	0[a]	56 ± 3	0[a]	0[a]	35 ± 3	29 ± 6	17 ± 1	19 ± 6
L- β- ABA	0[a]	0[a]	0[a]	0[a]	54 ± 5	0[a]	0[a]	39 ± 3	30 ± 4	19 ± 2	14 ± 4
D- norvaline	0[a]	0[a]	0[a]	0[a]	50 ± 3	0[a]	10 ± 2	33 ± 1	23 ± 1	15 ± 1	15 ± 4
L- norvaline	0[a]	0[a]	0[a]	0[a]	53 ± 3	0[a]	11 ± 2	36 ± 2	24 ± 1	18 ± 1	15 ± 4
β-alanine	0[a]	0[a]	0[a]	0[a]	52 ± 4	0[a]	0[a]	38 ± 2	27 ± 1	19 ± 2	13 ± 4
D- leucine	0[a]	0[a]	0[a]	0[a]	51 ± 4	2 ± 0	3 ± 1	34 ± 1	22 ± 1	11 ± 1	10 ± 3
L- leucine	0[a]	0[a]	0[a]	0[a]	45 ± 3	2 ± 0	5 ± 1	32 ± 1	22 ± 1	11 ± 1	10 ± 3
D- norleucine	0[a]	0[a]	0[a]	0[a]	43 ± 4	0[a]	7 ± 0	18 ± 2	12 ± 1	13 ± 1	17 ± 8
L- norleucine	0[a]	0[a]	0[a]	0[a]	41 ± 1	0[a]	5 ± 0	21 ± 1	15 ± 1	13 ± 1	14 ± 7
γ-ABA	0[a]	0[a]	0[a]	0[a]	66 ± 4	0[a]	0[a]	32 ± 2	28 ± 3	26 ± 2	19 ± 6
D- aspartic acid	13 ± 1	0[a]	0[a]	12 ± 1	55 ± 2	9 ± 0	7 ± 1	22 ± 2	31 ± 2	24 ± 1	12 ± 3
L- aspartic acid	14 ± 1	0[a]	0[a]	14 ± 1	59 ± 3	10 ± 0	8 ± 0	25 ± 1	34 ± 2	26 ± 2	13 ± 4
6-AHA	0[a]	0[a]	0[a]	0[a]	40 ± 3	0[a]	0[a]	22 ± 1	25 ± 1	25 ± 1	20 ± 5
D- glutamic acid	0[a]	0[a]	0[a]	6 ± 0	51 ± 4	0[a]	9 ± 0	29 ± 2	29 ± 1	31 ± 3	15 ± 3
L- glutamic acid	0[a]	0[a]	0[a]	6 ± 0	49 ± 3	0[a]	9 ± 1	25 ± 2	26 ± 2	32 ± 3	14 ± 4

[a] Complete degradation (A/A0 = 0).
[b] Enantiomeric separation not possible under chromatographic conditions.

trols, no amino acids were detected in augite (A1), basalt lava (B1) and nontronite (N1). Hence, the lack of amino acid detection in the A1, B1 and N1 experiments cannot be unequivocally interpreted as caused by degradation. For the remaining minerals of experiment 1, amino acid degradation was observed. In the case of enstatite (E1) all amino acids suffered complete degradation.

In experiment 2 (spiking solution containing 10 μM of each amino acid), gypsum (Gy2) was the mineral that, on average, preserved a greater proportion of amino acids, whereas amino acids on enstatite (E2) and basaltic lava (B2) were completely degraded (Fig. 5 and Table 1). Gypsum, olivine, montmorillonite and nontronite were the only minerals that preserved all amino acids (Table 1). Saponite prevented degradation of all amino acids except D, L-β-AIB (Table 1).

Results from experiment 3 (minerals spiked with a solution containing 25 μM of each amino acid) showed that amino acids were preserved (to different degrees) in all minerals (Fig. 5). The percentage of surviving amino acids for augite (A3), basaltic lava, (B3) enstatite (E3), hematite (H3) and labradorite (L3) were below 10% (Fig. 5 and Table 2). On average, amino acids were

Table. 2
Summary of the individual A/A0 ratios (in %) obtained for experiment 3 (spiking solution, 25 μM of each amino acid) where A is the amount of the remaining amino acids detected in simulated samples and A0 is the amount of amino acids detected in the control.

Individual amino acid (A/A0) vs mineral	Augite (A3)	Basaltic lava (B3)	Enstatite (E3)	Goethite (G3)	Gypsum (Gy3)	Hematite (H3)	Jarosite (J3)	Labradorite (L3)	Monmorillonite (M3)	Nontronite (N3)	Olivine (O3)	Saponite (S3)
α-AIB	16 ± 1	2 ± 0	8 ± 1	22 ± 2	0[a]	5 ± 1	43 ± 4	6 ± 1	17 ± 2	12 ± 1	12 ± 1	20 ± 1
D,L-isovaline[b]	13 ± 2	2 ± 0	6 ± 1	21 ± 2	0[a]	5 ± 1	44 ± 4	5 ± 1	13 ± 1	11 ± 1	8 ± 1	22 ± 2
D-alanine	6 ± 1	3 ± 1	5 ± 1	21 ± 3	11 ± 1	6 ± 1	32 ± 2	7 ± 1	24 ± 2	15 ± 2	13 ± 1	17 ± 1
L-alanine	5 ± 0	2 ± 0	4 ± 0	18 ± 2	7 ± 1	5 ± 1	28 ± 2	6 ± 1	21 ± 1	11 ± 1	12 ± 1	15 ± 1
D- valine	7 ± 0	3 ± 1	5 ± 1	24 ± 2	15 ± 2	8 ± 1	47 ± 3	8 ± 1	22 ± 2	16 ± 2	17 ± 1	24 ± 2
L- valine	7 ± 0	3 ± 0	5 ± 0	24 ± 1	12 ± 1	8 ± 1	46 ± 2	7 ± 0	20 ± 1	13 ± 1	15 ± 1	20 ± 2
Glycine	0[a]	0[a]	0[a]	31 ± 3	22 ± 2	7 ± 1	28 ± 4	9 ± 1	40 ± 2	19 ± 2	18 ± 2	15 ± 1
D- β- AIB	0[a]	0[a]	0[a]	29 ± 2	23 ± 3	0[a]	42 ± 5	19 ± 2	25 ± 2	31 ± 3	20 ± 2	18 ± 2
L- β- AIB	0[a]	0[a]	0[a]	33 ± 2	27 ± 3	0[a]	37 ± 5	19 ± 2	28 ± 2	30 ± 3	20 ± 3	17 ± 1
D- β- ABA	0[a]	0[a]	0[a]	28 ± 1	20 ± 1	7 ± 0	32 ± 4	9 ± 1	24 ± 2	24 ± 2	20 ± 2	15 ± 1
L- β- ABA	0[a]	0[a]	0[a]	29 ± 2	23 ± 2	8 ± 1	31 ± 3	9 ± 1	26 ± 2	24 ± 3	20 ± 2	13 ± 1
D- norvaline	6 ± 0	3 ± 1	5 ± 1	29 ± 2	20 ± 2	9 ± 0	50 ± 3	8 ± 0	26 ± 2	20 ± 1	23 ± 1	24 ± 2
L- norvaline	7 ± 0	4 ± 1	6 ± 0	32 ± 2	23 ± 1	10 ± 1	51 ± 3	9 ± 1	30 ± 2	19 ± 2	26 ± 2	21 ± 1
β-Alanine	0[a]	0[a]	0[a]	28 ± 2	24 ± 2	5 ± 0	24 ± 2	10 ± 1	31 ± 2	24 ± 2	17 ± 1	12 ± 1
D- Leucine	5 ± 0	3 ± 0	5 ± 0	29 ± 1	25 ± 1	7 ± 0	32 ± 3	5 ± 0	18 ± 1	13 ± 1	21 ± 1	12 ± 0
L- Leucine	5 ± 0	3 ± 0	5 ± 0	28 ± 1	24 ± 1	7 ± 0	29 ± 1	5 ± 0	19 ± 1	12 ± 1	19 ± 1	11 ± 0
D- norleucine	6 ± 1	5 ± 0	5 ± 0	26 ± 1	23 ± 1	8 ± 1	42 ± 2	8 ± 0	18 ± 2	18 ± 1	20 ± 2	20 ± 1
L- norleucine	9 ± 1	5 ± 0	5 ± 0	29 ± 1	25 ± 1	7 ± 1	45 ± 1	7 ± 0	22 ± 2	17 ± 1	23 ± 1	20 ± 1
γ-ABA	0[a]	0[a]	0[a]	37 ± 2	38 ± 5	10 ± 1	78 ± 3	10 ± 1	23 ± 1	39 ± 2	21 ± 1	18 ± 2
D- aspartic acid	5 ± 0	5 ± 0	6 ± 0	35 ± 3	33 ± 2	12 ± 1	32 ± 3	10 ± 0	16 ± 1	32 ± 3	26 ± 1	16 ± 1
L- aspartic acid	6 ± 0	7 ± 0	7 ± 1	40 ± 2	37 ± 2	14 ± 1	34 ± 4	11 ± 1	19 ± 1	35 ± 3	28 ± 1	18 ± 1
6-AHA	0[a]	0[a]	0[a]	35 ± 3	33 ± 3	8 ± 1	0[a]	12 ± 1	18 ± 1	28 ± 2	20 ± 1	22 ± 2
D- glutamic acid	0[a]	5 ± 0	7 ± 0	40 ± 4	32 ± 2	8 ± 1	40 ± 4	11 ± 0	15 ± 1	32 ± 2	26 ± 1	23 ± 2
L- glutamic acid	0[a]	5 ± 0	6 ± 1	37 ± 4	30 ± 2	8 ± 1	38 ± 2	10 ± 0	13 ± 1	29 ± 2	25 ± 1	22 ± 2

[a] Complete degradation (A/A0 = 0).
[b] Enantiomeric separation not possible under chromatographic conditions.

preserved most efficiently in jarosite (J3). Basaltic lava (B3) preserved the smallest amount of amino acids (Fig. 5).

The simulations using the minerals that were spiked with the 50 μM solution (experiment 4) reveal that nontronite (N4) preserved, on average, the largest proportion of amino acids (Fig. 5). The lowest percentage of surviving amino acids were found in augite (A4), basaltic lava (B4) and hematite (H4), with A/A0 values of 11%, 9% and 9%, respectively (Fig. 5).

In addition, our results indicate that amino acid enantiomers are degraded in the same degree (individual preservation ratios obtained for D- and L-amino acids enantiomers are provided in Tables 1–3). The average A/A0 calculated for all D and L enantiomers preserved after experiment 4 were 20.0 ± 1.1% and 20.4 ± 1.1%, respectively. In experiment 3, D-amino acids had an average A/A0 of 16.5 ± 1.2%, while L enantiomers had an average A/A0 of 16.7 ± 1.2%. Similarly, the average A/A0 ratios for D and L-amino acids obtained for experiment 2 were 17.3 ± 1.9% and 17.1 ± 1.9%, respectively.

3.2. BET analyses

The results obtained for the surface areas and pore sizes of the 11 minerals and basaltic lava used in the simulations are provided in Table 4. Surface area values range from 0.22 m^2/g (for basaltic lava) up to 129.01 m^2/g (for montmorillonite). Pore size values range from 5.17 nm in saponite up to 21.04 nm in olivine.

4. Discussion

The preservation from UV-induced degradation of amino acids spiked onto minerals is likely dependant on multiple factors. Here we analyze the results obtained from the simulations in light of the effect of 1) the structure of amino acids and 2) the physical/chemical features of the minerals that were used, in particular their ferric/ferrous iron content, surface area and pore size.

4.1. Effect of the amino acid structure

Decarboxylation induced by UV photolysis has been proposed as one of the main destruction pathways of amino acids (Bertrand et al., 2015; Boillot et al., 2002; Ehrenfreund et al., 2001; Johns and Seuret, 1970; ten Kate et al., 2005). Boillot et al. (2002) verified that L-leucine was subjected to decarboxylation under UV radiation. Furthermore, Ehrenfreund et al. (2001) suggested this mechanism to explain the destruction of amino acids such as glycine, alanine, α-aminoisobutyric acid and β-alanine under simulated conditions in interstellar gas and interstellar icy grains. Decarboxylation of amino acids by UV radiation results in the formation of a radical in the α-carbon atom (Ehrenfreund et al., 2001). The stability of the radical is dependent on the substituents bonded to the α-carbon atom. Alkyl substituent groups attached to the α-carbon atom contribute towards the stability of the resulting alkyl amine radical that forms after UV-induced decarboxylation and prolong the life of the amino acid (ten Kate et al., 2005). Therefore, we should expect that glycine (the simplest amino acid, with two hydrogen atoms bonded to the α-carbon) would be more degraded and have the lowest surviving ratios after the Mars-conditions simulation experiments. In fact, Li and Brill (2003) have shown that glycine has the highest relative aqueous decarboxylation rate when compared to the protein amino acids leucine, isoleucine, valine and alanine. In addition, we would expect that the amino acids more resistant to UV radiation and less prone to decarboxylation would be α-aminoisobutyric and isovaline, which are doubly substituted in the α-carbon. A group of our results agree with the overall effect of substitution in the α-carbon described above (Tables 1–3). For instance, glycine was less preserved than α-aminoisobutyric and isovaline in all augite, basaltic lava, enstatite and jarosite experiments 2, 3 and 4 (Tables 1–3). However, it is evident that the alkyl substituent groups are not the only factor contributing towards the stability of the amino acids. If that was the case, then isovaline and α-aminoisobutyric would be the most stable amino acids in our experiments and the ones with the highest A/A0 values, which is not observed in our results. Other amino acid

Table. 3
Summary of the individual A/A0 ratios (in %) obtained for experiment 4 (spiking solution, 50 μM of each amino acid) where A is the amount of the remaining amino acids detected in simulated samples and A0 is the amount of amino acids detected in the control.

Individual amino acid (A/A0) vs mineral	Augite (A4)	Basaltic lava (B4)	Enstatite (E4)	Goethite (G4)	Gypsum (Gy4)	Hematite (H4)	Jarosite (J4)	Montmorillonite (M4)	Nontronite (N4)	Olivine (O4)	Saponite (S4)
α-AIB	38 ± 4	22 ± 1	27 ± 3	34 ± 3	27 ± 1	9 ± 0	27 ± 3	33 ± 4	36 ± 2	11 ± 2	11 ± 1
D,L-isovaline[b]	34 ± 5	23 ± 1	26 ± 2	33 ± 3	27 ± 1	9 ± 0	31 ± 3	24 ± 3	40 ± 2	8 ± 1	8 ± 0
D-alanine	21 ± 3	10 ± 1	22 ± 2	26 ± 2	21 ± 2	9 ± 0	26 ± 2	34 ± 3	31 ± 2	11 ± 1	15 ± 1
L-alanine	17 ± 2	8 ± 1	19 ± 2	22 ± 2	17 ± 2	9 ± 1	22 ± 2	30 ± 3	27 ± 2	9 ± 1	12 ± 2
D- valine	15 ± 2	16 ± 1	39 ± 2	26 ± 2	22 ± 1	8 ± 1	22 ± 1	26 ± 2	46 ± 2	16 ± 1	19 ± 1
L- valine	14 ± 1	14 ± 1	37 ± 2	26 ± 2	20 ± 1	9 ± 1	24 ± 1	24 ± 1	44 ± 2	14 ± 1	17 ± 1
glycine	0[a]	4 ± 0	4 ± 1	26 ± 1	29 ± 2	13 ± 1	18 ± 2	41 ± 4	42 ± 1	15 ± 2	20 ± 1
D- β- AIB	0[a]	0[a]	18 ± 2	24 ± 2	22 ± 2	8 ± 0	20 ± 2	28 ± 1	30 ± 5	20 ± 2	25 ± 2
L- β- AIB	0[a]	0[a]	18 ± 2	25 ± 1	26 ± 2	9 ± 0	19 ± 1	31 ± 1	31 ± 3	23 ± 1	28 ± 1
D- β- ABA	0[a]	7 ± 0	23 ± 2	20 ± 1	19 ± 1	7 ± 0	16 ± 1	25 ± 1	34 ± 1	15 ± 1	23 ± 1
L- β- ABA	0[a]	9 ± 1	25 ± 3	21 ± 1	23 ± 2	7 ± 0	17 ± 1	24 ± 2	30 ± 2	17 ± 1	21 ± 1
D- norvaline	14 ± 1	15 ± 1	48 ± 1	29 ± 1	23 ± 1	9 ± 1	24 ± 1	28 ± 1	57 ± 3	18 ± 1	24 ± 1
L- norvaline	16 ± 1	17 ± 1	53 ± 3	32 ± 2	25 ± 1	11 ± 1	26 ± 1	30 ± 2	55 ± 3	20 ± 1	26 ± 1
β-Alanine	0[a]	0[a]	15 ± 2	20 ± 1	24 ± 1	15 ± 1	15 ± 1	29 ± 2	21 ± 1	14 ± 1	16 ± 1
D- leucine	9 ± 1	11 ± 0	35 ± 2	23 ± 1	17 ± 1	9 ± 1	24 ± 1	17 ± 1	31 ± 4	16 ± 1	17 ± 0
L- leucine	9 ± 1	11 ± 0	30 ± 3	25 ± 1	17 ± 1	10 ± 1	24 ± 2	17 ± 1	28 ± 3	14 ± 1	16 ± 0
D- norleucine	14 ± 1	15 ± 1	54 ± 2	20 ± 2	23 ± 1	8 ± 0	23 ± 2	19 ± 1	54 ± 3	18 ± 1	20 ± 1
L- norleucine	12 ± 1	16 ± 1	59 ± 3	24 ± 2	25 ± 1	10 ± 0	26 ± 1	22 ± 1	52 ± 2	20 ± 1	22 ± 1
γ-ABA	0[a]	7 ± 1	11 ± 1	18 ± 1	32 ± 2	6 ± 0	11 ± 1	22 ± 1	37 ± 3	21 ± 2	17 ± 1
D- aspartic acid	13 ± 1	4 ± 0	18 ± 2	21 ± 1	28 ± 1	13 ± 1	14 ± 1	16 ± 1	55 ± 3	17 ± 1	17 ± 2
L- aspartic acid	15 ± 1	5 ± 0	22 ± 2	23 ± 1	30 ± 1	15 ± 1	16 ± 1	18 ± 1	62 ± 4	19 ± 1	21 ± 2
6-AHA	0[a]	0[a]	9 ± 0	16 ± 1	28 ± 1	7 ± 1	9 ± 1	17 ± 1	29 ± 1	20 ± 1	16 ± 1
D- glutamic acid	9 ± 1	3 ± 0	11 ± 1	23 ± 1	34 ± 1	9 ± 1	20 ± 2	14 ± 1	54 ± 6	24 ± 2	14 ± 1
L- glutamic acid	9 ± 1	4 ± 0	10 ± 1	21 ± 1	34 ± 1	7 ± 1	17 ± 1	12 ± 1	55 ± 4	24 ± 1	13 ± 1

[a] Complete degradation (A/A0 = 0).
[b] Enantiomeric separation not possible under chromatographic conditions.

Table 4
Qualitative information on the iron content and its valence, as well as the surface area and pore size values from BET analyses for the minerals used in the Mars chamber simulations.

	Iron content	BET analyses	
		Surface area (m^2/g)	Pore size[a] (nm)
Augite	low Fe^{2+}	1.19 ± 0.01	12.91
Basaltic Lava	medium Fe^{2+}	0.22 ± 0.01	14.79
Enstatite	medium Fe^{2+}	0.50 ± 0.01	14.40
Goethite	high Fe^{3+}	2.13 ± 0.01	17.78
Gypsum	no iron	2.25 ± 0.01	12.01
Hematite	high Fe^{3+}	4.91 ± 0.04	11.51
Jarosite	high Fe^{3+}	4.98 ± 0.01	13.25
Labradorite	no iron	0.27 ± 0.01	17.11
Montmorillonite	low Fe^{3+}	129.01 ± 0.41	5.89
Nontronite	high Fe^{3+}	26.76 ± 0.24	7.36
Olivine	no iron	0.23 ± 0.01	21.04
Saponite	no iron[b]	37.26 ± 0.35	5.17

[a] Average pore width.
[b] Assessed from the XRD pattern.

structural and chemical factors (molecule dimensions and shape, pKa values, etc.) will affect the way of interaction or adsorption between the mineral surface and the amino acid. These factors probably also play a role in the stabilization of amino acids against UV light, but their complexity is beyond the scope of this article.

We observed that D and L amino acids were equally degraded in the simulations (Tables 1–3). This lack of enantiomeric preference regarding UV-induced degradation is consistent with the observations of Orzechowska et al. (2007) for D,L-aspartic acid, D,L-glutamic acid and D,L-phenylalanine.

4.2. Effects from the mineral features

The minerals can act as protectors of the amino acids from the UV radiation in several ways. First of all, the opacity of the mineral to UV radiation is a protection factor. Opacity increases approximately with the increasing average atomic number of the mineral. For the minerals investigated here, Fe is the only element with electrons in *d* orbitals, and is a much greater absorber of UV radiation than any of the other elements. Thus, as a good approximation, the presence of Fe can be considered the dominant factor controlling opacity to UV radiation. However, ferrous Fe promotes iron (II) catalyzed reactions that degrade organic molecules, and this is an important effect to be considered here. Other mineral protecting factors are a high specific surface area and small average pore space, both of which should allow for a greater proportion of the adsorbed amino acids to be protected from direct UV radiation. Table 4 provides the information on the above characteristics that can guide our discussion of their effect in the Mars simulation experiments. The chemical character of specific mineral adsorption sites may also have an effect in determining amino acid stability but they should be considered in conjunction with the chemical characteristics of the individual amino acid and are not discussed here.

4.2.1. Role of iron

Iron is a transition metal with UV-photoprotective properties (Olson and Pierson, 1986). The amount of ferric iron was found to be correlated with the ability of minerals to confer protection from UV-radiation (Hoang-Minh et al., 2010) and the protective role of ferric iron against UV radiation has been verified by Pierson et al. (1993), Gómez et al. (2003) and Gauger et al. (2015). In clay minerals, ferric iron increases the absorbance of UV radiation (Chen et al., 1979). Similarly, for sulfates, the opacity to UV radiation increases much from gypsum to jarosite (Martinez-Frias et al., 2006). In our experiments, two ferric iron-rich minerals, jarosite and nontronite (Table 4) had the highest amino acid preservation in experiments 3 and 4, respectively (Fig. 5). Within the smectite group, montmorillonite and nontronite preserved more amino acids than saponite, probably due to the absence of Fe in saponite (Table 4). The absence of Fe in saponite was inferred from X-ray diffraction data, because the position of the 060 peak at 1.534 Å indicates that Fe^{3+} is not present in any significant amount (Brown and Brindley, 1980). Poch et al. (2015) have suggested that nontronite not only

protects amino acids from UV light by shielding but that there is also a stabilizing interaction between the clay and the amino acids. These interactions perhaps help to dissipate absorbed energy or facilitate photodissociated molecules to recombine (Poch et al., 2015).

Of the two Fe oxides in our experiments, goethite had a good protection effect in experiments 3 and 4, as expected, but low in experiment 2, while hematite protection was always low (Fig. 5). These results highlight the fact that protection against UV radiation is controlled by a variety of phenomena. Watts et al., (1997) found that the combinations of hematite and hydrogen peroxide promote degradation of organic compounds. Goethite is also known to be a catalyst for iron (II) catalyzed reactions (Lin and Gurol, 1998), which contributes to the degradation of organic molecules. It is then possible that minerals where Fe is very abundant may promote electronic interactions between Fe atoms and adsorbed organic substances that cause their degradation. Thus, their overall effect of protection against UV is a balance between the electronic transfer effect and the UV-shielding effect.

4.2.2. Role of ferrous iron

Ferrous iron is known to degrade organic molecules in Mars-like conditions through iron (II) catalyzed reactions (Benner et al., 2000; Garry et al., 2006). Adsorbed water was removed from the mineral surfaces in our Mars chamber simulation experiments due to the low water vapor partial pressure (nominally zero), although traces may have remained in the smectites as these are the most hygroscopic of the minerals. Structural water or hydroxyls are not removed using our experimental procedure, but this is not relevant here because no mineral with ferrous iron contained structural water. For these reasons, iron (II) catalyzed reactions in our experiments most probably only involved ferrous iron in the minerals and the amino acids. Thus, it can be expected that minerals with ferrous Fe will have a degradation effect in our experiments. The balance between the degradation effect of Fe^{2+} and the UV-shielding effect of Fe will decide which of the two is manifested experimentally. Interestingly, Olson and Pierson (1986) observed that ferrous iron absorbs less UV radiation than ferric iron between 200 and 400 nm (the UV-range used in our simulations), and Chen et al. (1979) found that the UV absorption of nontronite decreased when ferric iron was reduced to ferrous iron. Therefore, the protective effect of Fe appears to be less effective in the case of ferrous iron. In our study, the generally low amount of surviving amino acids from the minerals containing ferrous Fe, augite, basaltic lava and enstatite (Table 4) is in agreement with ferrous iron being an important contributor for amino acid degradation under simulated Mars conditions. The basaltic lava includes three mineral phases containing ferrous iron: olivine, pyroxene and glass. The olivine used in this work is forsterite (Mg variety) according to XRD data and has little or no ferrous iron, which would explain the high amino acid preservation in comparison to augite, enstatite and basaltic lava. This explanation is compatible with the higher amino acid preservation in enstatite for experiment 4 (Fig. 5). The enstatite in our study is of the bronzite type, with low ferrous Fe content (10–30% $FeSiO_3$ in the $MgSiO_3$–$FeSiO_3$ series).

4.2.3. Surface area and pore size

According to Moores et al. (2007), the variation in small-scale geometries in the martian surface such as pits, trenches and overhangs would produce significant attenuation effects on the incident UV flux, and create safe spots for organisms and organic molecules to be preserved. A similar principle can be applied at the micro-scale for the minerals used in this work. Irregularities on the mineral surfaces will also create sites where organic molecules may be adsorbed and preserved from UV radiation. Higher surface areas in a mineral indicate smaller particle size and/or a higher amount of irregularities in the surface, both of which generate a higher number of sites where organic molecules can be protected from direct exposure to UV light.

In adsorption experiments, the key variable of the solid phase is the surface area: the larger the surface, the more adsorbate can be accommodated. Particle size is related to surface area, but is not the key variable, because surface area depends also on other variables. In our study, all the amino acid was forced to adsorb on the mineral surfaces and so there is no dependence between total amounts of amino acid adsorbed and surface area. The dependence is on how the amino acids were adsorbed and where, plus on the configuration of mineral particles in the well during the experiment, all of which affect exposure to radiation and resilience to it.

In addition to the surface area, the size of the pores should also influence the degradation of amino acids under a high flux of UV-radiation. Pores provide a site where organic molecules may be protected against radiation. The photoprotective effect conferred by the pores should be inversely correlated with their respective size. The range of pore size measured by BET is provided in Table 4. If all amino acids were able to penetrate the whole range of pores existent in our minerals, this would result that the smaller pores would create a more shielded environment for organic molecules by limiting the amount of UV influx in the site. On the contrary, bigger pores would let more radiation penetrate and induce more degradation.

From our results we observe that nontronite, montmorillonite and saponite were the minerals that had the highest surface areas and the smaller pore sizes (Table 4). Clay minerals of the smectite group have large surface areas and the ability to adsorb organic molecules both in external surfaces and in the space between the layers that make up the mineral structure (Mortland, 1970; Raussel-Colom and Serratosa, 1987). This fact is in agreement with the generally high amounts of amino acids preserved in nontronite, montmorillonite and saponite when compared to the other minerals (Fig. 5). With the clear exceptions of olivine and gypsum, the minerals with lower surface areas and larger pore sizes than the clays generally preserved less amino acids (Table 4, Fig. 5). Olivine, with a low surface area and the largest pore size, preserved more amino acids than labradorite, hematite, augite and basaltic lava, all of which have similar or larger surface areas and smaller pore sizes (Table 4). This is one more example that no single variable can explain amino acid preservation on the mineral surfaces and all variables have to be considered together in order to approach a correct interpretation.

4.3. Concentration effect

Overall, our results show that the concentration of amino acids in the experiments had an influence on amino acid preservation. The mineral displaying the highest photoprotective effect in each experiment varied with the amount of amino acids that were spiked into the minerals. Nontronite preserved the largest proportion of amino acids in experiment 4, whereas jarosite and gypsum did so in experiments 3 and 2, respectively (Fig. 5). In experiments 2, 3 and 4 the general trend is that amino acid preservation ratio increased with increasing spiking concentration. This was clearly observed in augite, basaltic lava, enstatite, hematite, labradorite and saponite (Fig. 5), although gypsum and montmorillonite are a clear exception to this trend, and the other minerals showed no specific trend (Fig. 5). However, if we consider that the lowest preservations occur in experiment 1, the trend of increasing preservation with increasing amino acid amounts in the mineral surfaces appears more robust. We provide tentative explanations to address these results that will need to be explored in future work.

The general increase of amino acid preservation with increasing spiking concentration may be related to the type of sites where

the amino acids were adsorbed. During the spiking procedure we let amino acids to adsorb to the mineral surfaces for 24 h and then the solution was evaporated. At lower concentrations of the amino acids, they probably adsorbed on the most available sites. As the concentration increased, probably the amino acids adsorbed in less exposed sites and thus more protected. This effect may have been enhanced by the experimental procedure. There are two obvious stages in the adsorption process. During the first step (adsorption in the suspension) the amount of water remains constant and there was an approach to equilibrium between amino acid in solution and in mineral sites. However, during the drying step the amount of water decreased rapidly and so increased the amino acid concentration in the existing water. This increasing concentration may have forced adsorption into the less exposed sites as the more exposed ones filled quickly.

Another plausible explanation for the increase of preserved amino acid with increasing spiking concentration may be based on the association of adsorbed amino acids on the mineral surfaces. As the amount of adsorbed amino acids increased, especially as the water dried, the amino acids may have entered in contact with each other more frequently on the mineral surface. Possible interactions between amino acids adsorbed in nearby sites may increase their stability and attenuate (in some way) the degradation induced by UV-radiation. Alternatively, some of the amino acids may have been adsorbed as aggregates, of which some molecules were exposed and some were covered by other molecules. This disposition would result in increased protection of the amino acids from UV radiation (Poch et al., 2014). However, we do not think that thick aggregates were likely to form given the low amino acid concentrations (0.1–5 μmol/g) and the available mineral surface (0.22–129 m^2/g, Table 4).

Gypsum is an interesting case in our experiments because it has a large preservation rate while it has no Fe, and neither its surface area nor its average pore size suggests an especially protective capacity (Table 4). In addition, gypsum preserved approximately two times more amino acids in experiment 2 than in experiments 3 and 4 (Fig. 5). Gypsum is a relatively soluble salt. It is expected that gypsum was partially dissolved during the 24 h contact with the spiking solution and that the dissolved gypsum recrystallized during the drying step of the spiking protocol. It is possible that recrystallization of dissolved calcium sulfate trapped or surrounded amino acids that were adsorbed on the remaining crystals. This putative entrapment of amino acids would have likely increased protection. If this entrapment occurred, its effect would probably have been more evident in the experiments using less concentrated spiking solutions (Fig. 5). This is because the relative amount of amino acids that were adsorbed during the 24 h contact between the solution and the gypsum was higher (as the total amino acid amount is lower, a greater proportion of it adsorbs early), and then also a higher proportion of them could be trapped by the crystallization during the later drying stage.

4.4. Implications for Mars exploration

In this work, clays and sulfate minerals proved to preserve, on average, more amino acids from UV-induced degradation than silicates, pyroxenes, iron oxides and feldspars. Precisely, the presence of clays and sulfate minerals on Mars is relevant in the astrobiology context because they indicate past habitable environments where water was present (Downs et al., 2015, Squyres et al., 2004). Clay minerals are associated with sites of accumulation and preservation of organic molecules due to their high adsorption capacity and their ability to preserve organic matter by stabilizing it and protecting it from oxidation (Mortland, 1970; Poch et al., 2015; Raussel-Colom and Serratosa, 1987). Sulfate minerals, such as jarosite and gypsum, may actually be opaque to UV radiation and protect life and respective biomarkers (Amaral et al., 2007; Aubrey et al., 2006; Hughes and Lawley, 2003). Because clays of the smectite group and sulfate minerals are (1) related to environments amenable to life and (2) good biomarker preservers, they should be targeted for the detection of organic molecules in future life-searching missions such as NASA's 2020 mission.

Olivine of forsterite composition also preserved considerable amounts of amino acids during the Mars simulation, despite its low surface area and high pore size. Olivine (including low iron varieties) is widely distributed on Mars (Ody et al., 2013). According to our results, forsterite and perhaps other olivine minerals of low Fe content might be considered good targets for the detection of life biomarkers on Mars, provided that there are geological clues towards possible habitable environments. However, despite the high amino acid preservation verified in our results, we believe that olivine should be less relevant for life and organic biomarkers searching missions due to its usual association with basaltic minerals that do not preserve high amounts of amino acids and high weathering susceptibility by water (Kuebler et al., 2003).

An important aspect of our experiments in relation to the search for biomarkers on Mars is the mineral ability for amino acid preservation at low amino acid content. Given the low concentrations of organic matter expected on Mars, gypsum, montmorillonite, nontronite, saponite and olivine appear as much better candidates to preserve amino acid biomarkers than the other minerals tested (Fig. 5). This fact adds one more reason to target smectite clays (nontronite, saponite, montmorillonite) and gypsum on Mars. For these minerals, their protective ability does not drop at 10 μM amino acid concentration, as appears to happen with the other Mars-relevant minerals. To further support our results, indigenous chlorinated hydrocarbons were detected by the Curiosity rover in the Yellowknife Bay formation on Mars (informally named the Sheepbed member), which contained ~20 wt% smectite clay (Ming et al., 2014; Vaniman et al., 2014).

The amino acid standards used in this experiment ranged from 0.1 μmol/g of mineral to 5 μmol/g, i.e. ranged from ~10 parts per million (ppm) to 500 ppm for each amino acid present in the mineral matrix. This range of values is quite high when compared to terrestrial Mars soil analogues. As an example, a typical Mars soil analogue from Atacama and Arequipa have individual amino acid concentration in the range of 1–10 ppb (e.g. Peeters et al., 2009), while Mars soil analogues richer in amino acids, such as Salten Skov and some Utah soils, range from 10 ppm to 50 ppm (Martins et al., 2011; Peters et al., 2009). The abundances used in this manuscript are higher than what it is expected to be present on Mars, placing a limit of detection for the preservation of amino acids under Mars conditions.

As a final note, UV irradiation on Mars is limited to the first millimeters, but energetic particles (solar energetic particles (SEP) and galactic cosmic rays (GCR)) can go deeper in the subsurface, reach organic molecules and contribute to their degradation. A SEP dose of 600–700 mGy/yr can reach the surface of Mars and penetrate to around 10 cm, while GCR are typically capable of penetrating up to 3 m into the subsurface (Parnell et al., 2007) and over geological time, deactivate spores and degrade organic species (Dartnell et al., 2007). Therefore, future work should study the influence of the minerals on the preservation of organic molecules under simulated Mars conditions using SEP and GCR.

5. Conclusions

We analyzed the UV-induced degradation of 25 amino acids spiked onto augite, basaltic lava, enstatite, goethite, gypsum, hematite, jarosite, labradorite, montmorillonite, nontronite, olivine and saponite under simulated Mars conditions. The results indicated that:

(1) D- and L-enantiomers were degraded in the same extent in all experiments.
(2) The proportion of amino acid preservation in each mineral tends to increase with the concentration of amino acids in the spiking solution. At the lowest concentration (1 μM or each amino acid) no amino acids were recovered due to a combination of complete degradation and low extractability.
(3) Results from the experiments at concentrations of 10, 25 and 50 μM (of each amino acid) show that, on average, smectite clays (montmorillonite, nontronite and saponite), sulfates (gypsum and jarosite) and olivine (forsterite) were the minerals that preserved more amino acids. Augite, basaltic lava, enstatite and hematite preserved the least proportions of amino acids.
(4) For the interpretation of the results, several major variables affecting protection from UV radiation were considered: a) amino acid molecular structure and substitution in the α-carbon; b) mineral opacity to UV light, driven mainly by Fe content; c) large surface area and small average pore size are likely to promote amino acid preservation; d) ferrous iron content promotes iron (II) catalyzed reactions and thus dissociation of amino acids. None of the above single variables can fully explain our results, but most of them can be related to one or more of these variables.
(5) Our results indicate that rocks with abundant smectite (montmorillonite, saponite, nontronite) and/or sulfates (gypsum, jarosite) are very good targets to search for amino acid biomarkers (and possibly other type of biomarkers) on Mars, due to the preserving ability of the above minerals, even at relatively low amino acid concentration (1 μmol/g). This argument is strengthened because the above minerals typically form in environments amenable to life. As a result, future missions that aim to detect organic molecules on the Red planet, such as the NASA 2020 mission should consider targeting locations rich in these minerals in order to maximize the chances of finding preserved martian organic molecules.

Acknowledgments

Renato dos Santos is funded by a Janet Watson Scholarship. Zita Martins is funded by a Royal Society University Research Fellowship (grant UF080820 and grant UF130324). The authors acknowledge financial support from STFC (grant ST/J001260/1). M. Patel acknowledges funding from STFC grant ST/I003061/1. We thank two anonymous reviewers for their insightful comments.

References

Amaral, G., Martinez-Frias, J., Vázquez, L., 2007. UV shielding properties of Jarosite Vs. Gypsum: Astrobiological implications for Mars. World App. Sci. J. 2, 112–116.
Arvidson, R.E., Squyres, S.W., Bell, J.F., et al., 2014. Ancient aqueous environments at endeavour Crater, Mars. Science 343, 1248097-1–1248097-8. doi:10.1126/science.1248097.
Aubrey, A.D., Cleaves, H.J., Chalmers, J.H., et al., 2006. Sulfate minerals and organic compounds on Mars. Geology 34, 357–360. doi:10.1130/G22316.1.
Benner, S.A., Devine, K.D., Matveeva, L.N., et al., 2000. The missing organic molecules on Mars. Proc. Nat. Acad. Sci. 97, 2425–2430. doi:10.1073/pnas.040539497.
Bertrand, M., Chabin, A., Colas, C., et al., 2015. The AMINO experiment: Exposure of amino acids in the EXPOSE-R experiment on the International Space Station and in laboratory. Int. J. Astrobiol. 14, 89–97. doi:10.1017/S1473550414000354.
Boillot, F., Chabin, A., Buré, C., et al., 2002. The perseus exobiology mission on MIR behaviour of amino acids and peptides in Earth Orbit. Orig. Life Evol. Biosph. 32, 359–385. doi:10.1023/A:1020501226958.
Brown, G., Brindley, G.W., 1980. X-ray diffraction procedures for clay mineral identification.. In: Brindley, G.W., Brown, G. (Eds.), Crystal Structures of Clay Minerals and their Identification. Mineral. Soc, London, pp. 305–360.
Chen, Y., Shaked, D., Banin, A., 1979. The role of structural iron (III) in the UV absorption by smectites. Clay Miner. 14, 93–102.
Cockell, C.S., Catling, D.C., Davis, W.L., et al., 2000. The ultraviolet environment of Mars: Biological implications past, present, and future. Icarus 146, 343–359. doi:10.1006/icar.2000.6393.
Cuadros, J., 2002. Structural insights from the study of Cs-exchanged smectites submitted to wetting-and-drying cycles. Clay Minerals 37, 473–486. doi:10.1180/0009855023730046.
Cuadros, J., Aldega, L., Vetterlein, J., et al., 2009. Reactions of lysine with montmorillonite at 80 °C: Implication for optical activity, H+ transfer and lysine-montmorillonite binding. J. Colloid Interf. Sci. 333, 78–84.
Dartnell, L.R., Desorgher, L., Ward, J.M., et al., 2007. Modelling the surface and subsurface martian radiation environment: Implications for astrobiology. Geophys. Res. Lett. 34, L02207-1–L02207-6. doi:10.1029/2006GL027494.
Des Marais, D.J., 2010. Exploring Mars for evidence of habitable environments and life. Proc. Am. Philosoph. Soc. 154, 402–421.
Downs, R.T., Science Team, MSL, 2015. Determining mineralogy on Mars with the CheMin X-Ray diffractometer. Elements 11, 45–50. doi:10.2113/gselements.11.1.45.
Ehlmann, B.L., Edwards, C.S., 2014. Mineralogy of the martian surface. Annu. Rev. Earth Planet. Sci. 42, 291–315. doi:10.1146/annurev-earth-060313-055024.
Ehrenfreund, P., Bernstein, M.P., Dworkin, J.P., et al., 2001. The photostability of amino acids in space. Astrophys. J. 550, L95–L99.
Fairén, A.G., Davila, A.F., Lim, D., et al., 2010. Astrobiology through the ages of Mars: The study of terrestrial analogues to understand the habitability of Mars. Astrobiology 10, 821–843. doi:10.1089/ast.2009.0440.
Freissinet, C., Glavin, D.P., Mahaffy, P.R., et al., 2015. Organic molecules in the Sheepbed Mudstone, Gale Crater, Mars. J. Geophys. Res.: Planets 120, 495–514. doi:10.1002/2014JE004737.
Garry, J.R.C., Loes Ten Kate, I., Martins, Z., et al., 2006. Analysis and survival of amino acids in martian regolith analogs. Meteorit. Planet. Sci. 41, 391–405. doi:10.1111/j.1945-5100.2006.tb00470.x.
Gauger, T., Konhauser, K., Kappler, A., 2015. Protection of phototrophic iron(II)-oxidizing bacteria from UV irradiation by biogenic iron(III) minerals: Implications for early Archean banded iron formation. Geology 43, 1067–1070. doi:10.1130/G37095.1.
Georgiou, C.D., Papapostolou, I., Sun, H., et al., 2007. Superoxide radical assays and applications in Mars-like Atacama soils. J. Geophys. Res. (Biogeosci.) 112, G04S13-1–G04S13-6. doi:10.1029/2006JG000390.
Georgiou, C.D., Sun, H.J., McKay, C.P., et al., 2015. Evidence for photochemical production of reactive oxygen species in desert soils. Nature Commun. 6, 7100-1–7100-11. doi:10.1038/ncomms8100.
Gómez, F., et al., 2003. UV radiation effects over microorganisms and study of protective agents. In: Proceedings of the Third European Workshop on Exo-Astrobiology. Madrid, Spain.
Grotzinger, J.P., et al., 2014. A habitable Fluvio-Lacustrine environment at Yellowknife Bay, Gale Crater. Mars. Sci. 343, 1242777-1–1242777-14. doi:10.1126/science.1242777.
Hassler, D.M., et al., 2014. Mars' surface radiation environment measured with the Mars science laboratory's curiosity rover. Science 343, 1244797-1–1244797-6. doi:10.1126/science.1244797.
Hoang-Minh, T., Le, T.L., Kasbohm, J., et al., 2010. UV-protection characteristics of some clays. Appl. Clay Sci. 48, 349–357. doi:10.1016/j.clay.2010.01.005.
Hughes, K.A., Lawley, B., 2003. A novel Antarctic microbial endolithic community within gypsum crusts. Environ. Microbiol. 5, 555–565. doi:10.1046/j.1462-2920.2003.00439.x.
Johns, R.B., Seuret, M.G., 1970. Photochemistry of biological molecules-III. Mechanism of photodamage of alanine peptides in the solid state. Photochem. Photobiol. 12, 405–417. doi:10.1111/j.1751-1097.1970.tb06071.x.
Kieffer, H.H., Martin, T.Z., Peterfreund, A.R., et al., 1977. Thermal and albedo mapping of Mars during the Viking primary mission. J. Geophys. Res. 82, 4249–4291.
Kminek, G., Bada, J.L., 2006. The effect of ionizing radiation on the preservation of amino acids on Mars. Earth Planet. Sci. Lett. 245, 1–5.
Kuebler, K.E., et al., 2003. A study of olivine alteration to iddingsite using Raman spectroscopy. In: Lunar Planet. Sci. Conf., XXXIV, p. 1953.
Li, J., Brill, T.B., 2003. Spectroscopy of hydrothermal reactions part 26: Kinetics of decarboxylation of aliphatic amino acids and comparison with the rates of racemization. Int. J. Chem. Kinet. 35, 602–610. doi:10.1002/kin.10160.
Lin, S.S., Gurol, M.D., 1998. Catalytic Decomposition of hydrogen peroxide on iron oxide: Kinetics, mechanism, and implications. Environ. Sci. Technol. 32, 1417–1423. doi:10.1021/es970648k.
Martinez-Frias, J., Amaral, G., Vázquez, L., 2006. Astrobiological significance of minerals on Mars surface environment. Rev. Environ. Sci. Biotechnol. 5, 219–231. doi:10.1007/s11157-006-0008-x.
Martins, Z., Sephton, M.A., Foing, B.H., et al., 2011. Extraction of amino acids from soils close to the Mars Desert Research Station (MDRS), Utah. Int. J. Astrobiol. 10, 231–238. doi:10.1017/S1473550410000431.
Martins, Z., Modica, P., Zanda, B., et al., 2015. The amino acid and hydrocarbon contents of the Paris meteorite: Insights into the most primitive CM chondrite. Meteorit. Planet. Sci. 50, 926–943. doi:10.1111/maps.12442.
Michalski, J.R., Bleacher, J.E., 2013. Groundwater activity on Mars and implications for a deep biosphere. Nat. Geosci. 6, 133–138. doi:10.1038/ngeo1706.
Ming, D.W., et al., 2014. Volatile and organic compositions of sedimentary rocks in Yellowknife Bay, Gale Crater, Mars. Science 343, 1245267-1–1245267-9. doi:10.1126/science.1245267.
Mortalnd, M.M., 1970. Clay-organic complexes and interactions. Adv. Agron 22, 75–117. doi:10.1016/S0065-2113(08)60266-7.
Moores, J.E., Smith, P.H., Tanner, R., et al., 2007. The shielding effect of small-scale martian surface geometry on ultraviolet flux. Icarus. Icarus 192, 417–433. doi:10.1016/j.icarus.2007.07.003.

Noblet, A., Stalport, F., Guan, Y.Y., et al., 2012. The PROCESS experiment: Amino and carboxylic acids under Mars-like surface UV radiation conditions in low-Earth Orbit. Astrobiology 12, 436–444. doi:10.1089/ast.2011.0756.

Ody, A., Poulet, F., Bibring, J.-P., et al., 2013. Global investigation of olivine on Mars: Insights into crust and mantle compositions. J. Geophys. Res. - Planets 118, 234–262. doi:10.1029/2012JE004149.

Olson, J.M., Pierson, B.K., 1986. Photosynthesis 3.5 thousand million years ago. Photosynth. Res. 9, 251–259. doi:10.1007/BF00029748.

Orzechowska, G.E., Goguen, J.D., Johnson, P.V., et al., 2007. Ultraviolet photolysis of amino acids in a 100 K water ice matrix: Application to the outer Solar System bodies. Icarus 187, 584–591. doi:10.1016/j.icarus.2006.10.018.

Parbhakar, A., Cuadros, J., Sephton, M.A., et al., 2007. Adsorption of L-lysine on montmorillonite. Colloids Surf. A 307, 142–149.

Parnell, J., Cullen, D., Sims, M.R., et al., 2007. Searching for life on Mars: Selection of molecular targets for ESA's Aurora ExoMars Mission. Astrobiology 7 (4), 578–604. doi:10.1089/ast.2006.0110.

Patel, M.R., Zarnecki, J.C., Catling, D.C., 2002. Ultraviolet radiation on the surface of Mars and the Beagle 2 UV Sensor. Planet. Space Sci. 50, 915–927.

Peeters, Z., Quinn, R., Martins, Z., et al., 2009. Habitability on planetary surfaces: Interdisciplinary preparation phase for future Mars missions. Int. J. Astrobiol. 8, 301–315.

Pierson, B.K., Mitchell, H.K., Ruff-Roberts, A.L., 1993. *Chloroflexus aurantiacus* and ultraviolet radiation: Implications for Archean shallow-water stromatolites. Orig. Life Evol. Biosph 23, 243–260. doi:10.1007/BF01581902.

Poch, O., Kaci, S., Stalport, F., et al., 2014. Laboratory insights into the chemical and kinetic evolution of several organic molecules under simulated Mars surface UV radiation conditions. Icarus 242, 50–63. doi:10.1016/j.icarus.2014.07.014.

Poch, O., Jaber, M., Stalport, F., et al., 2015. Effect of nontronite smectite clay on the chemical evolution of several organic molecules under simulated martian surface ultraviolet radiation conditions. Astrobiology 15, 221–337. doi:10.1089/ast.2014.1230.

Quinn, R.C., Martucci, H.F.H., Miller, S.R., et al., 2013. Perchlorate radiolysis on Mars and the origin of martian soil reactivity. Astrobiology 13, 515–520. doi:10.1089/ast.2013.0999.

Raussell-Colom, J.A., Serratosa, J.M., 1987. Reactions of clays with organic substances. In: Newman, A.C.D (Ed.), Chemistry of Clays and Clay Minerals. Mineral. Soc., pp. 371–422.

Ruff, S.W., Farmer, J.D., Calvin, W.M., et al., 2011. Characteristics, distribution, origin, and significance of opaline silica observed by the Spirit rover in Gusev crater, Mars. J. Geophys. Res. Planets 116 (E7), E00F23-1–E00F23-48. doi:10.1029/2010JE003767.

Squyres, S.W., Grotzinger, J.P., Arvidson, R.E., et al., 2004. Opportunity Rover's Athena science investigation at Meridiani Planum, Mars. Science 306, 1698–1703. doi:10.1126/science.1106171.

Squyres, S.W., Arvidson, R.E., Ruff, S., et al., 2008. Detection of silica-rich deposits on Mars. Science 320, 1063–1067.

Summons, R.E., Amend, Jan P., Bish, David, et al., 2011. Preservation of martian organic and environmental records: Final report of the Mars biosignature working group. Astrobiology 11 (2), 157–181. doi:10.1089/ast.2010.0506.

ten Kate, I.L., Garry, J.R.C., Peeters, Z., et al., 2005. Amino acid photostability on the martian surface. Meteorit. Meteorit. Planet. Sci. 40, 1185–1193. doi:10.1111/j.1945-5100.2005.tb00183.x.

Vaniman, D.T., et al., 2014. Mineralogy of a mudstone at Yellowknife Bay, Gale Crater, Mars. Science 343, 1243480-1–1243480-8. doi:10.1126/science.1243480.

Watts, R.J., Jones, A.P., Chen, P.-H., et al., 1997. Mineral-catalyzed Fenton-like oxidation of sorbed chlorobenzenes. Water Environ. Res. 69, 269–275. doi:10.2175/106143097X125443.

Westall, F., Loizeau, D., Foucher, F., et al., 2013. Habitability on Mars from a microbial point of view. Astrobiology 13, 887–897. doi:10.1089/ast.2013.1000.

Yen, A.S., Kim, S.S., Hecht, M.H., et al., 2000. Evidence that the reactivity of the martian soil is due to superoxide ions. Science 289, 1909–1912. doi:10.1126/science.289.5486.1909.